RESEARCH ACTIVITIES II
Department of Molecular Structure

II-A Laboratory and Astronomical Spectroscopy of Transient Molecules

Vast, cold, and low-density space environment is a unique laboratory, whose physical and chemical conditions are rarely attained in the laboratory on Earth. The unique space laboratory is favorable to the existence of transient molecules such as molecular ions, free radicals, and unstable molecules, most of which are very exotic and nonterrestrial. These exotic transient molecules are generally difficult and challenging problems for laboratory spectroscopy. Laboratory spectroscopy may be enriched by astronomical studies on non-terrestrial transient species which represent new developments in high-resolution molecular spectroscopy. On the other hand, detailed knowledge about new transient molecules obtained by laboratory spectroscopy is essential to a deeper understanding of physical and chemical processes in space. We developed a high-sensitivity submillimeter-wave and far-infrared spectrometers suitable for high-resolution spectroscopy of transient molecules of astronomical interest. We expect that our laboratory spectroscopy may accelerate the mutually beneficial aspect between laboratory spectroscopy, and astrochemistry and astrophysics.

II-A-1 Experimental Determination of the Ground-State Inversion Splitting in D_3O^+ by Microwave Spectroscopy

Mitsunori ARAKI *(Grad. Univ. Adv. Stud.)*, **Hiroyuki OZEKI and Shuji SAITO**

[*J. Chem. Phys.* **109**, 5707 (1998)]

The hydronium ion, H_3O^+, is one of the most fundamental species in aqueous acid-base chemistry and also in gas-phase interstellar chemistry. The ion is isoelectronic to ammonia showing an "umbrella inversion motion" and has been extensively studied spectroscopically. Liu and Oka[1] measured the crucial inversion separation in the $v_2 = 1$ state, $1^- \text{-} 1^+$, and derived the ground state splitting.

In the present study, inversion-rotation transitions of the fully deuterated hydronium ion, D_3O^+, were observed for the first time by microwave spectroscopy (see Figure 1). The ion was generated in a hollow cathode cell by dc-glow discharge of a mixture of D_2O and D_2. Twenty six P- and Q-branch transitions were measured precisely for the lowest pair levels of inversion motion in the frequency region of 220-565 GHz. The ground-state inversion splitting and effective molecular constants for the upper and lower levels were determined by a least-squares fit of the measured line frequencies. The inversion splitting was determined to be 15.3555044(45) cm^{-1}, where the number in parentheses denotes three standarad deviations of the fit. Furthermore, the inversion splitting in the $v_2 = 1$ state was calculated to be 191.3887(30) cm^{-1} from the present value, combined with IR band data by Petek et al.[2] The ground-state and $v_2 = 1$ state inversion splittings of D_3O^+ obtained in the present study are essential to a deep understanding of the inversion potential of H_3O^+.

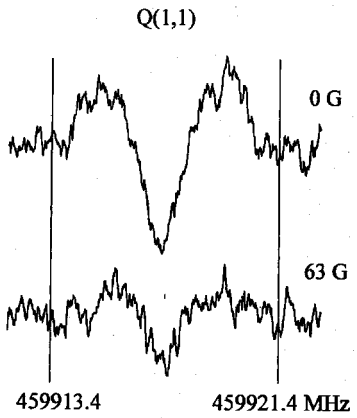

Figure 1. The Q(1,1) transition of D_3O^+. The integration time was 290 s (1600 scans). The upper trace was recoreded with no magnetic field, whereas the lower trace with a field of 63 G.

II-A-2 Microwave Spectroscopic Detection of a New Transient Phosphorus-Bearing Molecule, H_3PO

Imtiaz K. AHMAD, Hiroyuki OZEKI and Shuji SAITO

[*J. Chem. Phys.* **110** (1999) in press]

Experimental studies of simple intermediates in the oxidation of phosphorus are few in number. PH, PH_2, PO, PO_2, HPO, and H_2PO[1] have been studied and characterized mainly using microwave spectroscopy. There still remain several key and interesting transient molecules en route to the final product, H_3PO_4. The transient molecule H_3PO is such an example and has to date eluded gas-phase spectroscopic detection. Many sophisticated quantum chemical calculations so far carried out have concluded that its geometrical isomer H_2POH is more stable than H_3PO with an energy

References

1) D.-J. Liu and T. Oka, *Phys. Rev. Lett.* **54**, 1787 (1985).
2) H. Petek, D. J. Nesbitt, J. C. Owrutsky, C. S. Gudeman, X. Yang, D. O. Harris, C. B. Moore and R. J. Saykally, *J. Chem. Phys.* **92**, 3257 (1990).

difference of 6.5 kcal/mol,[2] though the trifluoride and trichloride of H_3PO are known to be symmetric-top molecules from their spectroscopic studies, and trialkylphosphines are easily changed into the corresponding phoshine oxides by autoxidation.

In the present study H_3PO was detected in the gas phase for the first time by using microwave spectroscopy. The spectral lines of H_3PO, which was generated by dc-glow discharge in a mixture of PH_3, CO_2 and H_2, showed a pattern clearly indicative of a symmetric top molecule. The observed rotational constants (see Table 1) of three isotopic species, H_3PO, D_3PO, and $H_3P^{18}O$, were used to determine the r_0 structure: $r_0(PO)$ = 1.4763 Å, $r_0(PH)$ = 1.4406 Å and HPO = 114.26˚. These strucural parameters deviate significantly from the most recent result predicted by ab initio calculations, and are compared and discussed with those of related molecules.

References

1) T. Hirao. S. Saito, and H. Ozeki, *J. Chem. Phys.* **105**, 3450 (1996).
2) J. A. Boatz, M. W. Schmidt and M. S. Gordon, *J. Phys. Chem.* **91**, 1743 (1987)

Table 1. Molecular Constants of H_3PO, D_3PO, and $H_3P^{18}O$ (MHz)[a,b]

Constant	H_3PO	D_3PO	$H_3P_{18}O$
B_0	17426.6217(20)	14599.8519(21)	16268.6646(22)
D_J	0.015205(13)	0.0104509(95)	0.013332(12)
D_{JK}	0.248390(87)	0.138966(56)	0.218681(75)
H_{JK}	0.0000054(13)	0.00000180(54)	0.00000490(87)

[a] MHz(3σ)
[b] The latest ab initio prediction, J. S. Kwiatkowski and J. Leszczynski, *J. Phys. Chem.* **96**, 6636 (1992): B = 17168.8860 MHz for H_3PO.

II-A-3 Microwave Spectrum of Silicon Trifluoride, SiF_3

Mitsutoshi TANIMOTO *(Shizuoka Univ. and IMS)* **and Shuji SAITO**

Silicon trifluoride SiF_3 is isovalent to CF_3 and one of rarely known symmeytric-top free radicals showing very complex fine and hyperfine structures in their rotational spectrum.[1] Transient SiF_3 and other members of SiF_n have been supposed to be important intermediate species in the silicon etching process. Stable SiF_4 and transient SiF and SiF_2 molecules have extensively been studied with various spectroscopic techniques. On the other hand, silicon trifluoride SiF_3 was investigated with matrix isolation IR spectroscopy as well as matrix and single crystal ESR spectroscopy. Gas phase spectrum was observed only in low resolution with UV-visible emission spectroscopy.

Previously we observed the microwave spectra of silicon trifluoride in the submillimeter region (300 GHz region) with a source modulation spectrometer by glow-discharging in 200 mTorr of Si_2F_6. The SiF_3 species yielded many spectral lines due to the spin-rotation and dipolar hyperfine interactions. In high frequency transitions many overlapping lines hindered the unambiguous K assignment. Subsequent observation of the rotational spectra down to the 105 GHz frequencies still did not allow the definite assignment of the hyperfine structures.

Recently we succeeded in observing the microwave spectrum in the 90 (N = 6-5) and 75 (N = 5-4) GHz regions with a spectrometer of improved sensitivity. In these transitions the K = 1 hyperfine components were found to show distinct splitting and thus the assignment of the K quantum number was made. It is found that the sign of the spin-rotation interaction constant is different from that of the iso(valence)electronic carbon trifluoride radical, CF_3 (Table 1).

Reference

1) Y. Endo, C. Yamada, S. Saito and E. Hirota, *J. Chem. Phys.* **77**, 3376 (1982).

Table 1. Molecular Constants of SiF_3 and CF_3[a]

Constant	SiF_3[b]	CF_3[c]
B_0	7509.0867(28)	10900.9118(52)
D_N	0.010014(28)	0.013882(87)
D_{NK}	-0.017118(30)	-0.02343(17)
D_K	0.0055(fixed)	
H_N (10^6)	0.329(93)	
H_{NK} (10^6)	-0.164(45)	
H_{KN} (10^6)	0.181(85)	
F_N (10^9)	-0.291(88)	
ε_{bb}	36.015(33)	-36.500(42)
ε_{cc}	4.766(108)	3.35(15)
a_F	386.57(118)	408.5(16)
T_{cc}	115.38(22)	320.01(20)
$T_{aa} - T_{bb}$	122.1(95)	40.1(49)

a MHz(2.5σ)
b Present study
c Reference 1.

II-A-4 The Pure Rotational Spectra of TiO($X^3\Delta$) and TiN($X^2\sum^+$)

Kei-ichi NAMIKI *(Grad. Univ. Adv. Stud. and Arizona State Univ.)***, Shuji SAITO, J. Scott ROBINSON** *(Arizona State Univ.)* **and Timothy C. STEIMLE** *(Arizona State Univ. and IMS)*

[*J. Mol. Spectrosc.* **191**, 176 (1998)]

The pure rotational transitions of TiO ($^3\Delta_r$) and TiN ($^2\Sigma^+$) have been observed in the 220-460 GHz spectral range with the submillimeter-wave spectrometer at IMS, as briefly reported in the former Annual Review.[1)] In addition, the two lowest rotational transitions of TiO at 63 and 94 GHz have been observed using molecular beam pump/probe microwave optical double resonance (PPMODR) technique. An improved set of spectroscopic parameters for TiO ($X^3\Delta_r$) was generated by combining the new PPMODR and submillimeter-wave absorption measurements. Similarly, an improved set of spectroscopic parameters for TiN ($X^2\Sigma^+$) was generated by combining the new submillimeter-wave absorption measurements with the previously recorded PPMODR measurements.[2)] The determined Δ-type doubling parameter for TiO ($X^3\Delta_1$) is effectively modeled using the fourth-order perturbation expression given by Brown et al.[3)]

References

1) K. Namiki, T. C. Steimle and S. Saito, *Ann. Rev.* II-A-6 (1996).
2) D. A. Fletcher, C. T. Scurlock, K. Y. Jung and T. C. Steimle, *J. Chem. Phys.* **99**, 4288 (1993).
3) J. M. Brown, A. S. -C. Cheung and A. J. Merer, *J. Mol. Spectrosc.* **124**, 464 (1987).

II-A-5 Microwave Spectrum of the PD_2 Radical in the $^2B_1$ Ground Electronic State

Tsuyoshi HIRAO *(Grad. Univ. Adv. Stud. and IMS)*, **Shin-ichi HAYAKASHI** *(Nagoya Univ.)*, **Satoshi YAMAMOTO** *(Univ. Tokyo)* **and Shuji SAITO**

[J. Mol. Spectrosc. **187**, 153 (1998)]

The PH_2 radical is isovalent to NH_2 and one of the fundamental bent triatomic free radicals in molecular spectroscopy. The PH_2 and NH_2 radicals are two examples showing the Renner-Teller effect in the nonlinear triatomic molecules. The NH_2 radical has been extensively studied by various high-resolution spectroscopic methods[1)] in the regions from optical to microwave, whereas spectroscopic studies on PH_2 have been relatively limited.

In the present study, the rotational spectrum spectrum of the PD_2 radical in the $^2B_1$ ground electronic state was measured to determine its force field and then the accurate r_z molecular structure PH_2 and PD_2. One hundred thirty fine and hyperfine components of 20 b-type rotational transitions were measured and analyzed by least-squares methods. The detailed molecular constants including the rotational constants, centrifugal distortion constants, the spin-rotation coupling constants, and the hyperfine coupling constants of both the phosphorus and the deuterium nuclei were precisely determined. The harmonic force field of PH_2 was derived from centrifugal distortion constants, inertial defects, and the reported vibrational frequencies for PH_2 and PD_2. The determined force field was used to make harmonic corrections to the observed moments of inertia, and the r_z structures for both species were derived:for PH_2, r_z(PH) = 1.43365(23) Å, and θ_z(HPH) = 91.622(32)˚, and for PD_2, r_z(PD) = 1.42852(17) Å, and θ_z(DPD) = 91.646(23)˚, where errors are due to residual inertial defects of the corrected moments of inertia.

References

1) M. Tonooka, S. Yamamoto, K. Kobayashi and S. Saito, *J. Chem. Phys.* **106**, 2563 (1997).

II-B Development of a Mt. Fuji Submillimeter-Wave Telescope

Shuji SAITO, Hiroyuki OZEKI, Hideo FUJIWARA, Satoshi YAMAMOTO *(Univ. Tokyo)*, **Yutaro SEKIMOTO** *(Univ. Tokyo)*, **Junji INATANI** *(National Space Developing Agency)*, **Masatoshi OHISHI** *(National Astronomical Observatory)* **and Norio KAIFU** *(National Astronomical Observatory)*

In recent years the submillimeter-wave to far infrared region has attracted much attention in the field of astronomy because the initial stage of star forming activity or in other words, the final stage of molecular cloud contraction shows various physical and chemical phenomena in the energy region of this wavelength. Several submillimeter-wave telescopes have now been developed to study astrophysics and astrochemistry of the star-forming regions through atomic and molecular spectral lines. Since atmospheric attenuation, mainly due to water vapor, becomes high in the submillimeter-wave to far infrared region, astronomical observations should be made at a high-altitude site with a cold environment.

We are building a submillimeter-wave telescope at the summit of Mt. Fuji. The main scientific purpose of our project is (1) a survey of the neutral carbon line at 492 GHz, and (2) a search for new simple and fundamental molecules, especially related to interstellar dust chemistry, which will help us to understand evolutionary physical and chemical processes of molecular clouds as a whole.

II-B-1 Development of a Backend System for Mt. Fuji Submillimeter Wave Telescope: An IF Band Synthesis Unit and a New Data Accumulator

Hiroyuki OZEKI, Hideo FUJIWARA and Shuji SAITO

The backend system of Mt. Fuji Submillimeter-wave telescope consists of a wideband acousto-optical spectrometer (AOS) and a data accumulator. Although this basic system has been developed and used since

October '97, it can be applied only to normal 'Position Switching' observation. To meet demands for various kind of observation, we are constructing two additional units for the backend system; one is an IF synthesis unit and the other is new data accumulator for OTF (on the fly) mapping.

The IF synthesis unit is an apparatus which enables one spectrometer to observe spectral lines of multiple frequency bands. In the present system, two IF signals coming from 345 GHz and 492 GHz SIS mixers are shaped with high-order band pass filters and are mixed to synthesize new IF signal by a diplexer. We will be able to observe both CO (J = 3-2, 345.796 GHz) and CI ($^3P_1$ - $^3P_0$, 492.161 GHz) emission lines simultaneously with the IF synthesis unit. This will contribute to investigate the physical evolution of molecular clouds to stars through an elucidation of the chemical evolution of carbon.

OTF (on the fly) mapping is an efficient method in survey observation, which is different from a conventional 'position switching' method. In OTF observation, the spectral data was acquired continuously with an antenna being swept the object to be observed in a constant velocity. Various overheads can be avoided in the observation process such as antenna positioning, observation efficiency is expected to be greatly improved. A new type of data accumulator must be necessary which can process a huge amount of spectral data ejected continuously from the AOS. The new data accumulator is equipped with analog-to-digital converters and ultra-fast interface units to take raw data. The processed spectral data will be shared with a host computer by NFS in which the client and the host are directly connected with 100Mbps network. The data acquisition program of the data accumulator is accessible through the network, and can be further developed after the installation of the system to the telescope site. This is fairly convenient for such a telescope that the site is difficult of access in the winter season.

II-C Laser Cooling and Trapping of Neutral Atoms

When an atom absorbs or emits a photon, the atom is accelerated or decelerated because a photon has momentum. On the other hand, a strong radiation field modifies the internal energy of an atom, so that an atom in an inhomogeneous radiation field receives a force from the field. The former mechanism allows us to decrease the translational temperature of neutral atoms down to an extremely low temperature by laser radiation, and the latter enables the spatial control of neutral atoms with lasers. As the translational temperature goes down to the nano kelvin region, the atomic de Broglie wavelength becomes a macroscopic size, and macroscopic quantum-mechanical collective motion of atoms can then be expected to occur. The long de Broglie wavelength also enables us to realize an atomic interferometry. On the other hand, easy control of atomic spatial position and velocity with lasers is expected to open the possibility of various applications. For these reasons, we have been studying the laser cooling and trapping of neutral atoms.

II-C-1 Isotopic Differences in Rate Coefficients of Cold Penning Collisions between Optically Trapped Metastable He Atoms

Mitsutaka KUMAKURA and Norio MORITA

We have confined about 10^5 triplet metastable ^{4}He and ^{3}He atoms separately in magneto-optical traps at a temperature of 0.5 mK and number density of 10^9 cm^{-1}, and have measured rate coefficients of cold Penning collisions between the trapped atoms ($He^* + He^* \rightarrow He^+ + He + e^-$) by counting ions produced in the traps. In cold collisions, collisional processes can considerably be modified by near-resonant laser light. To obtain both modified and unmodified rate coefficients, ions produced in the presence and absence of trapping laser light have been counted by turning the trap laser on and off repeatedly. By fitting a phenomenological rate equation for ionization to the atomic density dependence of ion count rates, the unmodified rate coefficient has been determined to be $(3.8 \pm 1.1) \times 10^{-10}$ cm^3/s for ^{4}He and $(1.1 \pm 0.4) \times 10^{-9}$ cm^3/s for ^{3}He (denoted by k_4 and k_3, respectively), and the modified ones are $(2.1 \pm 0.6) \times 10^{-8}$ cm^3/s for ^{4}He and $(3.5 \pm 1.3) \times 10^{-8}$ cm^3/s for ^{3}He (denoted by k_4^M and k_3^M, respectively). The ratios k_3/k_4 and k_3^M/k_4^M are about 2.9 and 1.7, respectively, and the former ratio is much larger than the latter, which is almost equal to the one expected for the normal temperature collision. Moreover, the ratios k_3^M/k_3 and k_4^M/k_4 are about 32 and 55, respectively, and the latter ratio is much larger than the former. To understand these remarkable isotopic differences, we have theoretically calculated the rate coefficients, examining the number of potentials for colliding helium atoms. The calculated rate coefficients k_3, k_4, k_3^M, and k_4^M are 1.0×10^{-9} cm^3/s, 2.0×10^{-10} cm^3/s, 1.3×10^{-8} cm^3/s, and 1.1×10^{-8} cm^3/s, respectively, and these are all in good agreement with the experimental values. Through this calculation, it has been found that only s-waves can contribute to the unmodified Penning collision at this cold temperature owing to the presence of high centrifugal barriers for higher partial waves, and a large isotopic difference in the number of the s-waves that can contribute to the ionization results in the remarkable difference between k_3 and k_4, which is unclear because of averaging over many partial waves at a normal temperature or in the presence of the laser-modification.

II-D Spectroscopy of Ions and Atoms in Liquid Helium

Ions and atoms in liquid helium are known to reside in bubble-like cavities due to the Pauli repulsive force between electrons. Physical properties in these exotic surroundings are determined by the potential energy of impurity-He_n system, the surface tension energy of the liquid helium, and the pressure-volume energy. Spectroscopic study of ions in liquid helium is expected not only to give information on the structure and dynamics of the bubbles, but also to contribute to the study on the property of superfluid liquid helium. Moreover, if ions are trapped in liquid helium by a radio-frequency trap or just below the liquid helium surface by a static electronic field, this kind of study is expected to break a new way in the experimental physics of low temperature and low dimensional plasma.

II-D-1 Laser Spectroscopy of Yb^+ Ions in Liquid Helium

Yoshiki MORIWAKI and Norio MORITA

Although spectroscopic observations of many neutral atoms in liquid helium have so far been demonstrated, there have been no such observations on ions other than Ba^+. This may be because of difficulties in optical detection of ions in liquid helium: for example, low density of foreign ions due to the Coulomb repulsion between the ions and also due to recombination with electrons, and low detection efficiency due to extraordinarily broadened spectra. However, the first difficulty can be overcome by implanting ions in liquid helium with laser sputtering of a metal tip in a strong electric field, which is applied to prevent ions from recombination with electrons. With this method, we have successfully observed emission and absorption spectra of the $4f^{14}6s^2S_{1/2}$ - $6p^2P_{1/2}$ (D1) and $4f^{14}6s^2S_{1/2}$ - $6p^2P_{3/2}$ (D2) transitions of Yb^+. Properties of the observed spectra are as follows: (1) The excitation spectrum of the D1 transition shows some broadening and blue shift in comparison with those of free ions. The shift and width of the emission spectrum are smaller than those of the excitation spectrum. (2) The excitation spectrum of the D2 transition is doubly peaked. In addition, the emission from the $4f^{14}6p^2P_{1/2}$ state is clearly observed after the excitation to the $4f^{14}6p^2P_{3/2}$ state. The fine structure splitting in the $4f^{14}6p^2P_j$ state of Yb^+ (3330 cm^{-1}) is expected to be much larger than the interaction potential between the Yb^+ ion in the $4f^{14}6p^2P_j$ state and the He atom, and this means that an ion bubble in the $4f^{14}6p^2P_{1/2}$ state is spherical. An ion bubble in the $4f^{14}6s^2S_{1/2}$ state is, of course, also spherical, so that a simple model for transitions between spherical bubbles can explain property (1). On the other hand, a vibration of the ion bubble in a deformed mode leads to energy level splitting in the $4f^{14}6p^2P_{3/2}$ state (dynamic Jahn-Teller effect). The splitting of the excitation spectrum of the D2 transition (property (2)) can be explained by this picture. However, transitions between the $4f^{14}6p^2P_j$ states have not been clearly understood yet. The ^2P state of Yb^+-He is expected to have a potential minimum, as is the case in the pair state of alkali-He. After the excitation to the $4f^{14}6p^2P_{3/2}$ state, the He atom approaches the potential minimum point. If some relaxation occurs at the potential minimum, the D1 emission spectrum should be more broadened and its center wavelength should be more red shifted than the observed ones. This is because the interaction between Yb^+-He is so large at the minimum point that, instead of spherical bubble formation, an exciplex is expected to be formed. Therefore transitions between the $4f^{14}6p^2P_j$ states are expected to occur in a very early stage after the ^2P state is created, and this means that the transition rate between the $4f^{14}6p^2P_j$ states is considerably large. For further analysis, detailed theoretical calculations on the Yb^+-He potential are necessary.

II-D-2 Laser Spectroscopy of Yb atoms in Liquid Helium

Yoshiki MORIWAKI and Norio MORITA

Spectra of the Yb atom in liquid helium have been observed. It has been found that excitation spectra of the $4f^{14}6s^2\ ^1S_0$ - $4f^{14}6s6p\ ^1P_1$ and $4f^{14}6s^2\ ^1S_0$ - $4f^{13}(^2F_{7/2})5d_{5/2}6s^2(7/2,5/2)_1$ transitions show extremely small spectral width (~ 0.1nm), while in other atoms in liquid helium spectral widths are usually very large. For the latter transition, this property can be explained by the fact that electrons in inner shells are shielded by outer electrons with respect to the perturbation caused by surrounding helium atoms. On the other hand, it needs further analyses to explain the spectrum of the former transition, in which a valence electron is excited.

II-D-3 Theoretical Analyses of the Spectrum of Mg Atoms in Liquid Helium

Yoshiki MORIWAKI and Norio MORITA

In our previous experiment, it was found that the emission spectrum of the $3s3p\ ^1P_1 \rightarrow 3s^2\ ^1S_0$ transition of Mg atoms in liquid helium shows an extraordinary broadening and a large red-shift in comparison with atomic bubble transitions so far observed. This cannot be explained by the usual bubble model in which a continuous bubble interface is assumed. We have instead proposed an exciplex formation model, in which we assume that He atoms localize near the Mg atom in the nodal plain of the $3p$ electron and form a ring structure. Minimization of the total energy has shown that the most probable form of the exciplex is Mg-He_{10}. By using the spectral method, we have calculated an emission spectrum of the transition from this exciplex to the bound free ground state. As a result, it has been found that the shift is well explained, and that this model provides much improvement in the spectral broadening in comparison with the bubble model. This means that the exciplex model is more suitable for understanding the dynamics in the $3s3p\ ^1P_1 \rightarrow 3s^2\ ^1S_0$

transition than the bubble model does. This is the first evidence for the formation of exciplexes in a ring-like structure. We have also calculated emission spectra of the same type exciplexes of Na, Mg^+, and Ca^+ in the np^2P_j state. This will be helpful in the experimental search for spectra of these atoms and ions in liquid helium, which have not been observed yet.

II-E Structure and Function of Respiratory Terminal Oxidases

In the aerobic respiratory chain of *Escherichia coli*, there are structurally unrelated two terminal oxidases. A heme-copper oxidase, cytochrome *bo* is predominantly expressed under highly aerated growth conditions while an alternative oxidase, a putative heme-heme oxidase, cytochrome *bd*, is predominant under microaerobic conditions. Both oxidases catalyze the two-electron reduction of ubiquinol-8 and the four-electron reduction of dioxygen, whereas only cytochrome *bo* exhibits vectorial proton transport. However, only a little structural information has been given for these ubiquinol oxidases. To clarify the molecular mechanism of electron transfer, chemical reaction of dioxygen, and proton pumping in the two respiratory terminal oxidases, we utilize various molecular spectroscopic techniques (*e.g.*, resonance Raman, EPR, FTIR) in conjuction with methods of molecular biology and biochemistry.

II-E-1 Fluoride-Binding to the Oxidized *Escherichia coli bd*-Type Ubiquinol Oxidase Studied by Visible Absorption and EPR Spectroscopies

Motonari TSUBAKI *(Himeji Inst. Tech. and IMS)*, **Tatsushi MOGI** *(Univ. Tokyo)* **and Hiroshi HORI** *(Osaka Univ.)*

Escherichia coli produces cytochrome *bo*- and *bd*-type ubiquinol oxidases, both of which reduce molecular oxygen to water, whereas only *bo*-type oxidase exhibits vectorial proton transport. It is believed that the *bd* type oxidase contains two heme *b* centers (heme b_{558} and heme b_{595}) and one heme *d* center. To clarify the structure of the reaction center, we analyzed the purified *bd*-type oxidase in oxidized state with visible absorption and EPR spectroscopies using fluoride ion as a monitoring probe. The observed visible spectral changes upon fluoride-binding (blue shifts of high-spin charge-transfer bands from 743 and 595 nm to 708 and 575 nm, respectively) were typical of those observed for other ferric iron-chlorin species, indicating that fluoride ion binds at the ferric heme *d* center. In EPR spectra, fluoride-binding to the oxidized enzyme caused a complete disappearance of low-spin signals and a formation of a rhombic high-spin signal at g = 6.3, 5.5, and 2.00. Each component of the high-spin signal showed a doublet (with splitting of 3.5, 2.9, and 10.8 mT, respectively) which arises from interaction of the unpaired spin of iron with the nuclear magnetic moment of ^{19}F, which has a spin of one-half.[1),2)] This unexpected result establishes that the rhombic high-spin signal previously assigned to ferric heme b_{595} is actually derived from the ferric heme *d* center.

References

1) H. Morimoto and M. Kotani, *Biochim. Biophys. Acta* **126**, 176 (1966).
2) J. Peisach, W. E. Blumberg, S. Ogawa, E. A. Rachmilewitz and R. Oltzik, *J. Biol. Chem.* **246**, 3342 (1971).

II-E-2 Azide- and Cyanide-Bindings to the *Escherichia coli bd*-Type Ubiquinol Oxidase Studied by Visible Absorption, EPR and FTIR Spectroscopies

Motonari TSUBAKI *(Himeji Inst. Tech. and IMS)*, **Tatsushi MOGI** *(Univ. Tokyo)* **and Hiroshi HORI** *(Osaka Univ.)*

To clarify the structure of the reaction center of *bd*-type ubiquinol oxidase, we analyzed the oxidized enzyme with visible absorption, EPR and FTIR spectroscopies using azide and cyanide ions as monitoring probes. Azide-binding to the oxidized enzyme caused a formation of a new EPR low-spin signal characteristic to low-spin ferric iron-chlorin-azide species. In the g6 region, there was no appreciable change. In visible absorption spectra, a disappearance of high-spin charge-transfer bands (595 and 643 nm) and an appearance of a new band at 650 nm were observed. These results suggest that the primary binding site of azide is the heme *d* center. FTIR spectra gave a new bound azide antisymmetric stretching band at 2010.5 cm^{-1}, presumably derived from a low-spin species. This azide band showed anomalies upon azide [^{15}N]-isotopic substitution, suggesting some effects from surrounding protein residues or from heme b_{595} in close proximity. The bound azide infrared band disappeared completely upon addition of cyanide. The visible spectral change upon cyanide-binding was typical of those observed for ferric iron-chlorin species with diol substituents in macrocycles. However, we could not observe any corresponding low-spin EPR signal. Instead, a derivative-shaped signal at g = 3.19 was observed. This unusual signal could be arising from the heme $d(Fe^{3+})$-CN-heme $b_{595}(Fe^{3+})$ moiety. Thus, the present study confirmed our previous proposal[1)] that heme *d* and heme b_{595} forms a binuclear metal center.

Reference

1) M. Tsubaki, H. Hori, Mogi, T. Mogi and Y. Anraku, *J. Biol. Chem.* **270**, 28565 (1995).

II-F Biomolecular Science

Elucidation of a structure-function relationship of metalloproteins is a current subject of this group. The primary technique used for this project is the stationary and time-resolved resonance Raman spectroscopy monitored by near IR to UV lasers. The main themes that we want to explore are (1) mechanism of oxygen activation by enzymes, (2) mechanism of active proton translocation and its coupling with electron transfer, (3) coupling mechanism of proton- and electron transfers by quinones in photosynthetic reaction center, (4) higher order protein structures and their dynamics, and (5) reactions of biological NO. In category (1), we have examined a variety of terminal oxidases, cytochrome P450s, and peroxidases, and also treated their enzymatic reaction intermediates by using the mixed flow transient Raman apparatus and the Raman/absorption simultaneous measurement device. For (2) the third generation UV resonance Raman (UVRR) spectrometer has been constructed and we are going to use it to the peroxy and ferryl intermediates of cytochrome c oxidase. In (3) we succeeded in observing RR spectra of quinones A and B in bacterial photosynthetic reaction centers for the first time and in assigning them with Raman spectra of electronically reduced isotope-labeled quinones. For (4) we developed a novel technique for UV resonance Raman measuremnts based on the combination of the first/second order dispersions of gratings and applied it successfully to 235-nm excited RR spectra of several proteins including mutant hemoglobins and myoglobins. Nowadays we can carry out time-resolved UVRR experiments with nanosecond resolution to discuss protein dynamics. We have succeeded in isolating the spectrum of β37-Trp and α42-Tyr of Hb A separately and their changes upon quaternary structure transition. For (5) we purified soluble guanylate cyclase from bovine lung, characterized it and observed its RR spectra.

II-F-1 Resonance Raman Characterization of Nitrosylheme in Myoglobin and Its Mutants

Takeshi TOMITA *(Grad. Univ. Adv. Stud.)*, **Shun HIROTA** *(Nagoya Univ.)*, **Takashi OGURA, John S. OLSON** *(Rice Univ.)* **and Teizo KITAGAWA**

Resonance Raman spectra have been observed for wild-type nitrosylmyoglobin (MbNO) and H64G, H64L, L29W, V68W, and V68T mutants at neutral and acidic pH. Raman excitation in resonance with the Soret band enabled us to detect the Fe-NO (ν_{Fe-NO}) and N-O stretching (ν_{NO}) and Fe-N-O bending (δ_{FeNO}) bands of nitrosylmyoglobins. The ν_{Fe-NO}, δ_{FeNO}, and ν_{NO} bands of wild type sperm whale MbNO at neutral pH were observed at 560, 452, and 1613 cm^{-1}, respectively, and substitution of the distal His64 to Gly or Leu caused an upshift of ν_{NO} to 1633 ~ 1636 cm^{-1} but no change in ν_{Fe-NO}. This change in ν_{NO} for the substitution is due to removal of hydrogen bonding between His64 and bound NO. Substitution of Leu29 with tryptophan altered ν_{Fe-NO} but caused no change in ν_{NO} at neutral pH. These properties are somewhat similar to those in MbO_2 but contrast with those of MbCO, for which the Fe-CO and C-O stretching frequencies have an inverse linear correlation. In the case of L29W-MbNO, the change in ν_{Fe-NO} is probably caused by tilting of the Fe-N bond from the heme normal due to steric hindrance with the large indole ring but not by changes in the Fe-N-O bond angle. When pH is lowered below 4, Mb(II)NO adopts the five-coordinate structure due to cleavage of the Fe-His bond. Accordingly, the Raman maker bands, ν_3 and ν_{10}, shift from 1500 and 1636 cm^{-1} at pH 7.4 to 1509 and 1646 cm^{-1} at pH 4 which are in agreement with those of a five-coordinate Fe-proto-porphyrin-NO complex in detergent micelles at neutral pH. The ν_{Fe-NO} and ν_{NO} bands of acidic MbNO are observed at 520 and 1668 cm^{-1} and exhibit no shift when the distal His is replaced by Gly or Leu. The latter observation supports previous X-ray crystallographic, infrared, and resonance Raman spectroscopic measurements which show that the distal histidine becomes protonated at pH 4 and swings out into the solvent away from the bound ligand.

II-F-2 Infrared Evidence for Cu_B Ligation of Photodissociated CO of Cytochrome *c* Oxidase at Ambient Temperatures and Accompanied Deprotonation of a Carboxyl Side Chain of Protein

Tadashi IWASE *(Grad. Univ. Adv. Stud.)*, **Constantinos VAROTSIS** *(Crete Univ. and IMS.)*, **Kyoko SHINZAWA-ITOH** *(Himeji Inst. Tech.)*, **Shinya YOSHIKAWA** *(Himeji Inst. Tech.)* **and Teizo KITAGAWA**

FTIR "light" minus "dark" difference spectra were measured for the CO complex of bovine fully reduced cytochrome *c* oxidase in H_2O and D_2O. Unexpectedly, the CuB-bound CO was identified at ambient temperatures in the photo-steadystate only for the D_2O solution, and simultaneously a difference peak was observed at 1737 cm^{-1}, indicating that the lifetime of the Cu_BCO is much longer in D_2O than in H_2O and that deprotonation of a carboxylic side chain occurs upon photodissociation of CO from heme a_3. However, the frequency and intensity of the CO stretching band remained unchanged in H_2O and D_2O between pH 6.8 and 9.2. Time-resolved IR diode laser spectrophotometry demonstrated that the protein structural changes have finished within the response time of the instrument (3 ms).

II-F-3 Interaction of Phosphatidylinositol 3-Kinase SH3 Domain with Its Ligand Peptide Studied by Absorption, UV Resonance Raman and Circular Dichroism

Nobuyuki OKISHIO *(Kanazawa Univ.)*, **Ryuji FUKUDA** *(Kanazawa Univ.)*, **Masako NAGAI** *(Kanazawa Univ.)*, **Shigenori NAGATOMO and Teizo KITAGAWA**

Absorption, UV resonance Raman and circular dichroism (CD) spectroscopies were applied to examine selectively the environmental and structural changes of Trp and Tyr residues in the binding cleft of phosphatidylinositol 3-kinase (PI3K) SH3 domain induced by ligand association. Comparison of the spectra of PI3K SH3 in the presence or absence of its ligand peptide RLP1 (RKLPPRPSK) indicated that RLP1 binding placed Trp55 of the SH3 in a polar environment and disrupted its H-bonding, and made Tyr residues to form a new H-bond in a hydrophobic environment. The D21N mutant (Asp21 changed to Asn) of the SH3 yielded the near-UV CD distinct from that of the wild-type, and its spectral changes induced by RLP1 were smaller and different compared with those of the wild-type, suggesting that the mutation of conserved Asp21 affected the conformation of the ligand affinity. These data provide a direct evidence for the occurrence of some environmental and structural alterations in the binding cleft of PI3K SH3 by the ligand association and the D21N mutation.

II-F-4 Quaternary Structure Sensitive Tyrosine Residues in Human Hemoglobin: UV Resonance Raman Studies of Mutants at α140, β35 and β145 Tyrosine

Masako NAGAI *(Kanazawa Univ.)*, **Henri WAJCMAN** *(Hopital Hneri Mondor)*, **Anges LAHARY** *(CHRU of Rousen)*, **Takashi NAKATSUKASA** *(Osaka Univ.)*, **Shigenori NAGATOMO and Teizo KITAGAWA**

Recent studies noted the contribution of α42 Tyr to the T-R dependent UV resonance Raman (UVRR) spectral changes of HbA [M. Nagai et al.; *J. Mol. Struct.* **379**, 65-75 (1996); Huang, et al. *Biochemistry* **36**, 6197-6206 (1997)], but the observed UVRR changes of Tyr residue can not be fully interpreted by α42 Tyr alone. To identify the remaining contributions the 235-nm excited UVRR spectra of mutant Hbs at α140, β35, and β145 were investigated here. The Fe-His stretching mode demonstrated that all these mutant Hbs take the T structure in the deoxy form under the present experimental conditions. UVRR change of Trp residue of these mutants upon the T-R transition was the same as that in HbA, indicating that the T-R dependent UVRR change of β37 Trp is not due to stacking with Tyr residues but is owing to changes in the surrounding hydrophobicity. Recombinant Hb (β35Tyr → Phe) gave an identical UVRR spectrum with that of Hb A, indicating that β35Tyr is not responsible. In the spectra of des(β146His, β145Tyr)Hb with IHP, the frequenccy shift of Tyr RR bands was the same as that in HbA but the intensity enhancement in the CO-form was small, suggesting that β145Tyr contributes partly to the intensity change, but scarcely relates to the frequency shift. In the spectra of Hb Rouen (α140Tyr → His), the frequency shifts of bands at 1617 (Y8a) and 1177 (Y9a) cm^{-1} following ligation were half of those in HbA, while the intensity enhancement was not detected. This results indicates that α140Tyr is resposible for both the frequency shift and the intensity changes. It is sugggested that the frequency shift of Tyr RR bands on the T → R transition is due to the changes of hydrogen bonding state of α42 and α140 Tyr, the intensity enhancement is due to the environmental chage of the penultimate Tyr in both α and β subunits (α140 and β145).

II-F-5 A Superoxodicopper(II) Complex Oxidatively Generated by a Reaction of Di-μ-Hydroxodicopper(II) Complex with Hydrogen Peroxide

Masahito KODERA *(Doshisha Univ.)*, **Yoshimitsu TACHI** *(Nagoya Univ.)*, **Shun HIROTA** *(Nagoya Univ.)*, **Kou KATAYAMA** *(Tokyo Inst. Tech.)*, **Hisashi SHIMAKOSHI** *(Tokyo Inst. Tech.)*, **Koji KANO** *(Tokyo Inst. Tech.)*, **Kiyoshi FUJISAWA** *(Tokyo Inst. Tech.)*, **Yoshihiko MORO-OKA** *(Tokyo Inst. Tech.)*, **Yoshinori NARUTA** *(Kyushu Univ.)* **and Teizo KITAGAWA**

[Chem. Lett. 798 (1998)]

Di-μ-hydroxodicopper(II) complex with a hexapyridine dinucleating ligand, $[Cu_2(OH)_2(hexpy)](CF_3SO_3)_2$ (hexpy = 1,2-bis[2-bis(2-pyridyl)methyl)-6-pyridyl]ethane), reacts with H_2O_2 in $MeCN/CH_2CL_2$ to give a superoxodicopper(II) complex. Its visible absorption (Figure 1) and resonanace Raman spectra (Figure 2) were observed.

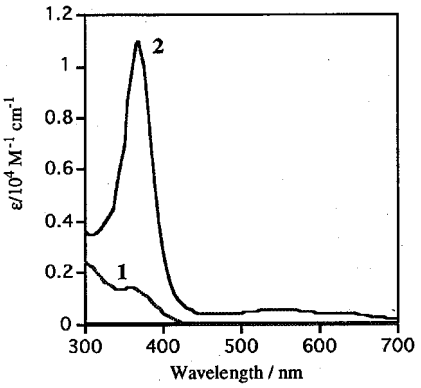

Figure 1. UV-vis spectra of **1** and **2** in $MeCN/CH_2CL_2$ (1:9, v/v) at-40˚C.

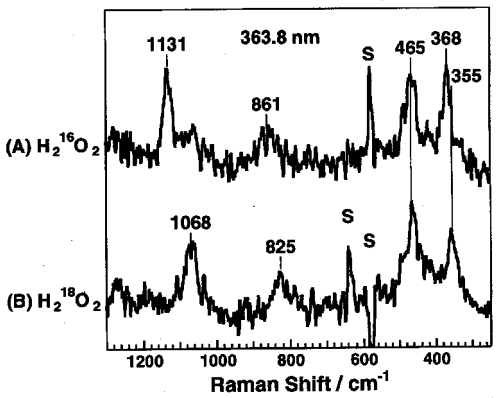

Figure 2. Resonance Raman spectra of **2** generated by the reaction of **1** with (A) $H_2{}^{16}O_2$ and (B) $H_2{}^{18}O_2$ in MeCN /CH_2Br_2 (1:9, v/v) at -30˚C. **S** denotes solvent (CH_2Br_2) bands.

II-F-6 Structural and Spectroscopic Characterization of a Mononuclear Hydroperoxo-Copper(II) Complex with Tripodal Pyridylamine Ligands

Akira WADA *(Nagoya Inst. Tech.)*, **Manabu HARATA** *(Nagoya Inst. Tech.)*, **Koji HASEGAWA** *(Nagoya Inst. Tech.)*, **Koichiro JITSUKAWA** *(Nagoya Inst. Tech.)*, **Hideki MASUDA** *(Nagoya Inst. Tech.)*, **Masahiro MUKAI, Teizo KITAGAWA and Hisahiko EINAGA** *(Nagoya Inst. Tech.)*

[*Angew. Chem. Int. Ed.* **37**, 798 (1998)]

Hydroperoxo-copper species are key intermediates in biological oxidations catalyzed by copper enzymes such as dopamine β-hydroxylase, glactose oxidase and superoxide dismutase. To confirm the structural characterization of the Cu(II)-OOH^- species, we prepared a mononuclear copper complex with a new designed tripodal pyridylamine ligand, bis(6-pivalamide-2-pyridylmethyl)-(2-pyridylmethyl)amine (bppa) and subjected it to reaction with hydrogen peroxide. Here we present the first example of an isolated copper-hydroperoxo species, $[Cu(II)(bppa)-(OOH^-)]^+$. The resonance Raman spectra of the reaction product of $Cu(bppa^-)]ClO_4$ with excess H_2O_2 in MeCN excited at 441.6 nm gave a strong Raman band at 856 cm^{-1}, which shifted to 810 cm^{-1} when ^{18}O-labeled H_2O_2 was used. Accordingly, the oxygen-isotope sensitive band is assigned to an O-O stretch of a hydroperoxo species. The crystal structure of this compound was also analyzed.

II-G Fast Dynamics of Photoproducts in Solution Phases

Picosecond time-resolved resonance Raman (ps-TR^3) spectroscopy is a promising technique to investigate ultrafast structural changes of molecules. However, this technique has not been used as widely as nanosecond TR^3 spectroscopy, mainly due to the lack of light source which has suitable repetition rates of pulses and wavelength tunability. In order to obtain qualified TR^3 spectra, first we need two independently tunable light sources for pump and probe pulses. Second, the repetition rate should be higher than kilohertz to keep a moderate average laser power without allowing the photon density of probe pulse too high. We succeeded in developing light sources for ps-TR^3 spectroscopy having wide tunability and kHz repetition, and applied them to study fast dynamics of photo-excited molecules. For carbonmonoxy myoglobin (MbCO), vibrational relaxation with the time costant of 1.9 ps was observed for CO-photodissociated heme. For Ni-octaethylporphyrin in benzene, different population rises in vibrationally excited levels were observed in the anti-Stokes spectra for different vibrational modes. For the same molecule in piperidine, coordination of two solvent molecules was observed in the transient (d,d) excited state. Nanosecond time-resolved Raman spectra were investigated for photodissociation of various mutant myoglobins. The UV ns-TR^3 experiments on MbCO demonstrated the presence of a transient open form of the ligand pathway.

II-G-1 Photo-Induced Solvent Ligation to Nickel(II)-Octaethylporphyrin Probed by Picosecond Time-Resolved Resonance Raman Spectroscopy

Yuki UESUGI *(Grad. Univ. Adv. Stud.)*, **Yasuhisa MIZUTANI and Teizo KITAGAWA**

[*J. Phys. Chem. A* **102**, 5809 (1998)]

Pump/probe picosecond time-resolved resonance Raman spectra of nickel(II)-octaethylporphyrin (NiOEP) in pyridine were observed in the time range -5 to 1000 ps. The spectra demonstrate generation of the vibrationally and electronically excited (d,d) state (B_{1g}) immediately after the excitation to the $\pi\pi^*$ state of the macrocycle, subsequent vibrational relaxation, and the formation of six-coordinate exciplex, $B_{1g}(L)_2$ (L: pyridine). Singular value decomposition analysis was applied to a series of picosecond time-resolved Raman spectra to investigate whether a five-coordinate complex was generated prior to the formation of the six-coordinate species. The results indicate insignificant population of the five-coordinate species preceeding the formation of $B_{1g}(L)_2$ and suggest concerted coordination of two solvent molecules to axial positions of the (d,d) excited NiOEP. The formation process of the $B_{1g}(L)_2$ species is discussed.

II-G-2 Time Resolved Resonance Raman Evidence for the Exciplex Formation of Free-Base Porphyrin with an Electron Acceptor

Anandi L. VERMA *(North-Eastern Hill Univ.)*, **Shin-ichiro SATO** *(JAIST)* **and Teizo KITAGAWA**

[*Chem. Phys. Lett.* **267**, 507 (1997)]

Pump/probe time-resolved resonance Raman experiments (TR^3) on free-base tetraphenylporphyrin (H_2TPP) in benzene and benzene plus CCl_4 mixed solvents were carried out to probe the mechanistic details and transient species involved in the photo-oxidation of H_2TPP. We have detected spectral features due to the π-radical cation, and exciplex tansient species in the singlet and triplet excited states at different time-scales in the presence of CCl_4 under laser irradiation. A mechanism for the photooxidation of porphyrins is discussed.

II-G-3 Comment on: Polarization Effects in Time Resolved Incoherent Anti-Stokes Raman Spectroscopy

Yasuhisa MIZUTANI

[*J. Chem. Phys.* in press (1998)]

The theoretical inspection on anti-Stokes Raman measurements following strong vibrational excitation by Hofmann et al. [M. Hofmann, R. Zürl and H. Graener, *J. Chem. Phys.* **105**, 6141 (1996)] was reexamined. It is found that the depolarized intensity is dependent on the incident angle of the pump pulse in the case of perpendicularly polarized pumping. Therefore one can observe "rotation-free" depolarized scattering only with some particular incident angle, which was not described in their paper. In addition to that, it is suggested to use the definition of depolarization ratio for polarized probe light instead of that for unpolarized light, since currently laser is a light source for this kind of experiments.

II-G-4 Saturation Raman Spectrosocpy as a Tool for Studying the Excited States of Complex Organic Molecules: Application to Nickel Octaethylporphyrin

Sergei G. KRUGLIK *(B. I. Stepanov Inst. and IMS)***, Alexander G. SHVEDKO** *(B. I. Stepanov Inst.)* **and Teizo KITAGAWA**

[*Asian J. Phys.* in press]

The nanosecond saturation resonance Raman (RR) technique has been reviewed and its peculiarities have been examined on the basis of a well-known molecular system, nickel octaethylporphyrin [Ni(OEP)] in solution. The results of mathematical treatment of saturation RR spectra of Ni(OEP) in weakly coordinating pyridine solvent suggest that the quantum yield of photogeneration of the six-coordinate Ni(OEP)(pyridine)$_2$ species is low, with the rate of complexation process being about one tenth of the rate of excitation deactivation within the manifold of four-coordinate species.

II-H Molecular and Electronic Structures of Metallofullerenes and the Fullerene Radical Anions

The continued interest in radical ions of fullerenes and metallofullerenes has resulted from the discovery of superconductivity in the CT complexes of alkali metals with fullerenes. Spectroscopic information concerning the molecular structure of the metallofullerene of La@C_{82} has been obtained by EPR and ENDOR measurements. From the comparison between the two results some dynamics of La metal ion within the carbon cage were also deduced.

II-H-1 ENDOR Measurements of La@C_{82}

Tatsuhisa KATO, Kazunobu SATO *(Osaka City Univ.)***, Takeji TAKUI** *(Osaka City Univ.)***, Deanna HURUM** *(Univ. Rochester)***, Robert W. KREILICK** *(Univ. Rochester)***, Shingo OKUBO** *(Niigata Univ.)* **and Takeshi AKASAKA** *(Niigata Univ.)*

^{13}C enriched La@C_{82} (^{13}C-La@C_{82}) sample was produced by the conventional arc-discharge procedure with electrodes of ^{13}C enriched LaC composite rods. The most abundant isomer of La@C_{82} was purified by a two stage HPLC purification procedure with Buckyprep and PBB columns. The ENDOR spectrum of toluene solution of La@C_{82} observed at 200 K is shown in the figure, and the most intense peak at 3.7 MHz was assigned to the ENDOR signal of ^{139}La nucleus, and several peaks between 3.75 MHz and 6.25 MHz to ^{13}C nuclei at the different site of the C_{82} cage. The ENDOR spectrum due to ^{13}C nuclei was well reproduced by the simulation with the ^{13}C hfc constants, as shown by a stick diagram and by a dotted line in the figure. The simulation is consistent with that for the ^{13}C satellite of the ESR spectrum for natural La@C_{82}. The ENDOR measurements could also indicate the dynamics of La metal ion inside the carbon cage. The ENDOR spectrum observed at the lower magnetic field exhibit relatively smaller ^{139}La peak than that at higher field. The fact reflects on the different relaxation rate for ^{139}La and ^{13}C.

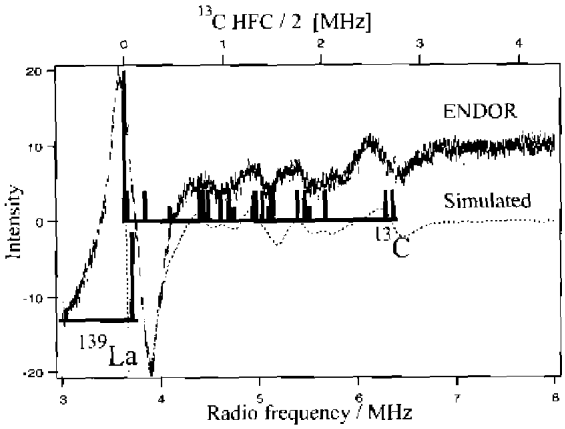

Figure 1. The ENDOR spectrum of toluene solution of purified ^{13}C enriched La@C_{82} (^{13}C-La@C_{82}) sample observed at 200 K. A stick diagram and a dotted line are the simulation with the ^{13}C hfc constants.

II-I Site Selective Spectroscopy in Solid Crystals

The line broadening due to the variation of the environment over the some sites in the crystal structure prevents from determining small energy splitting between pair of closely spaced levels with high accuracy. However the

broadening effects give a nice prove to investigate the intermolecular interaction in the crystal structure. On the other hand some techniques of the site selective spectroscopy to eliminate the disturbance were proposed. We are applying the technique of the heterodyne detection of optical magnetic double-resonance to some systems of crystal.

II-I-1 Coherent Raman Spectroscopy of Nuclear Quadrupole Resonance of La around Pr^{3+} in LaF_3

Michio MATSUSHITA, Akiko MUTOH *(Kitasato Univ.)* **and Tatsuhisa KATO**

[*Phys. Rev. B* **58** in press (1998)]

Coherent Raman spectroscopy was applied for an optical-rf double resonance study of LaF_3 crystal doped with Pr^{3+}. The coherent nuclear spin Raman scattering was detected as a function of the applied rf frequency. Exciting the resonance condition of the $^3H_4 \rightarrow {}^3P_0$ transition of Pr^{3+} (20925 cm^{-1}), only the La nuclei surrounding the Pr^{3+} ion were observed through their nuclear quadrupole resonance (NQR). The double resonance between the optical transition of the ion and the NQR transition of its neighboring nucleus is theoretically described by analyzing the magnetic dipolar interaction that is affected by the optical excitation. Under a certain restriction, which the present system fulfills, the intensity of the Raman heterodyne signal can be described by an analytical function of the internuclear vector and the orientation of the electric field gradient (EFG) at the Pr and La nuclei. Five different neighboring La nuclei were observed. They are different from the bulk La in both magnitude and orientation of the EFG. In addition, it was found that the laser frequency jitter affects the relative signal intensity of the different La NQR transitions through the optical pumping of the La spin levels.

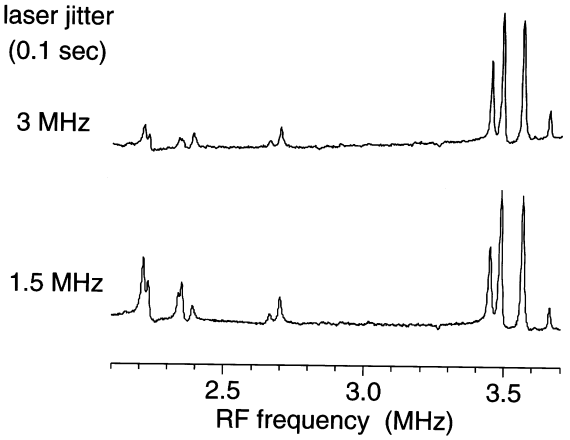

Figure 1. Influence of the laser frequency jitter on the Raman heterodyne signals. Comparison of the spectra between jitter of 3 MHz and 1.5 MHz. The NQR transitions whose frequencies are below the laser jitter are suppressed due to the optical pumping effect on the La spins.

II-I-2 Coherent Raman Scattering from a Delocalized Excitation in Molecular Crystal of 1,4-Dibromonaphthalene

Michio MATSUSHITA and Tatsuhisa KATO

Since its first application to NMR study of Pr^{3+} in LaF_3 in 1983, coherent Raman spectroscopy has been almost exclusively applied to rare earth impurity ions in inorganic crystals. The technique was for the first time shown to be applicable to magnetic resonance study of delocalized excitation in a molecular crystal. Optical-RF double resonance of the triplet exciton in 1,4-dibromonaphthalene (20192 cm^{-1}) was detected as coherent Raman scattering. One of the ESR transitions of the triplet exciton and the NQR transitions of ^{79}Br and ^{81}Br in the excited state were observed. The structure of the ESR transition and the intensity of the NQR transitions reflect the nature of the exciton through the hyperfine interaction between the delocalized electron spin and the Br nuclear spins.

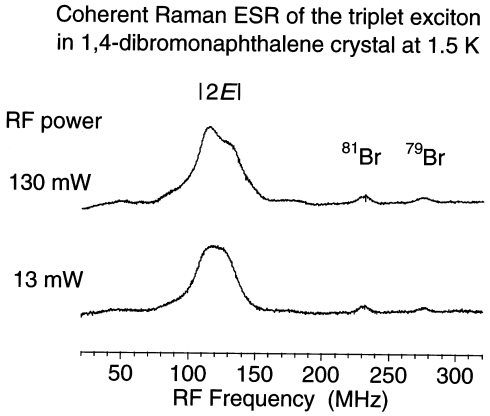

Figure 1. Raman heterodyne detected zero-field magnetic resonance of the triplet exciton in 1,4-dibromonaphthalene at 1.5 K. A cw laser was tuned to excite the triplet exciton at 20192 cm^{-1} (495.2 nm) and coherent Raman scattering was measured as a function of the frequency of the applied RF. Transition around 120 MHz is the $|2E|$ ESR transition of the triplet exciton. The transitions at 232 and 276 MHz are the NQR transitions of ^{81}Br (I = 3/2) and ^{79}Br (I = 3/2) in the exciton state, respectively.

II-J State Correlated Raman Spectroscopy

The vibrational Raman polarizability tensor responds to molecular reorientational relaxation process, and the structural environment in condensed media. The measurement of Raman scattering is a powerful technique for the study of molecular motion and of the mechanism of phase transition. We've built up the system of multichannel type detection of Raman scattering combined with the temperature controlled cell.

II-J-1 Polarized Raman Scattering Measurements of MHPOBC

Naoki HAYASHI and Tatsuhisa KATO

Polarized Raman scattering was measured on the successive smectic phase, SmA, SmC_α*, SmC*, SmC_γ* and SmC_A* of MHPOBC. 2nd and 4th order parameters of the Raman tensor, $<P_2>$ and $<P_4>$, were evaluated. The C=C stretching mode of phenyl rings and C=O stretching modes of carbonyl groups in core and chiral parts of each smectic phase were investigated. The tilt angle for spiral axis was taken into consideration for the analysis of the order parameters. $<P_2>$ and $<P_4>$ obtained were plotted with respect to the temperature. It was noticed that the values of the order parameters, especially of $<P_4>$, exhibited considerable dip at the temperature range of the SmC* phase. It is supposed that the molecular ordering was influenced by the ferroelectric molecular interaction. Moreover $<P_4>$ obtained for the C=O stretching mode of chiral CO group showed a prominent decrease comparing with the others, while $<P_2>$ showed a similar change. This fact suggests the specific dynamics for the chiral CO group in the process of the transition around SmC* phase.

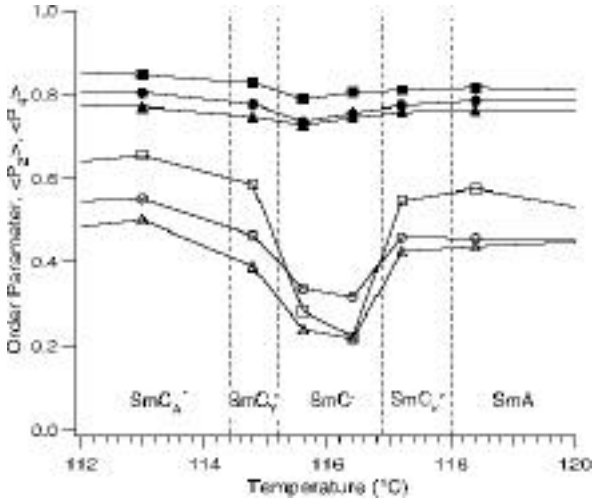

Figure 1. The order parameters of $<P_2>$ and $<P_4>$. ■: $<P_2>$ for the chiral C=O, □: $<P_4>$ for the chiral C=O, ●: $<P_2>$ for the phenyl C=C, ○: $<P_4>$ for the phenyl C=C, ▲: <P2> for the core C=O, △: $<P_4>$ for the core C=O.

II-K Double Resonance Spectroscopy Using Two Phase-Locked Lasers

Optical-Optical double resonance (OODR) is one of the most sophisticated techniques in high resolution spectroscopy. It is as precise as microwave spectroscopy and provides detailed information which is often complementary to other spectroscopic information. Most of OODR experiments observe change of the population induced by irradiation of two laser fields resonant with two transitions of a three level system. However, if we could control the phase relation between the two laser fields and could detect phase dependent signals, it would give direct information on the phase in the quantum state excited by two phase-controlled coherent radiations. In order to perform this coherent OODR experiment, we are developing a light source system where the difference frequency between two lasers is kept phase-1ocked to a microwave frequency standard.

II-K-1 Direct Observation of the Quantum Phase Induced by Third-order Nonlinear Susceptibility Using Phase-Locked OODR Spectroscopy

Motohiro KUMAGAI *(Tokyo Inst. Tech.)*, **Hideto KANAMORI** *(Tokyo Inst. Tech. and IMS)*, **Michio MATSUSHITA and Tatsuhisa KATO**

Optical-optical double resonance (OODR) is one of most sophisticated techniques in high-resolution spectroscopy. Two laser radiation makes a coherent quantum state in materials. However, most of OODR experiments have observed only the change in the population among the three levels interacting with the two lasers. If we utilize coherency of the quantum system, we can get direct information on the phase of the quantum state.

We have been developing a phase-locked OODR spectrometer using two CW single mode lasers. All the components of experimental system are schematically shown in Figure 1. The difference frequency of two Titanium-sapphire ring lasers was phase-locked to a tunable MW frequency standard. A hyper-fine structure in the D_2 line of Rubidium atom in a Zeeman cell was coherently excited by these master and slave radiation. The optical beat signal after the interaction with the atoms was detected by a high speed photodiode, and the phase shift from the original optical beat was picked up by a double balanced mixer. Figure 2. shows cosine and sine components of the optical beat signal obtained by the phase sensitive detection. The narrower structures with sub-Doppler width appeared in the upper and lower traces correspond to the imaginary and the real part of the third order nonlinear susceptibility, respectively.

This quantum phase monitoring technique in the frequency domain will be developed further for studies of dephasing process in an excited molecule and phase controlled reaction dynamics.

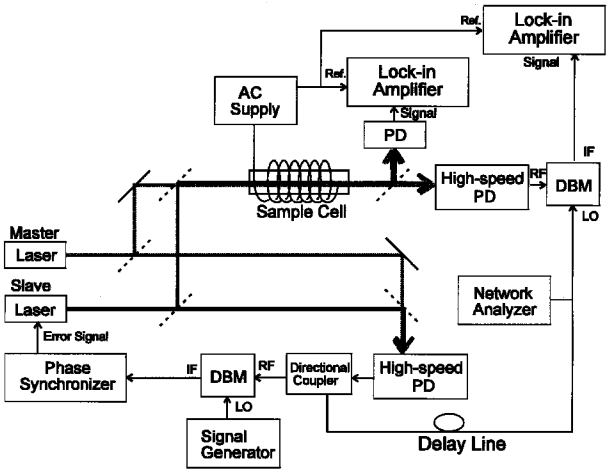

Figure 1. Block diagram of phase-locked OODR spectroscopy system. Zeeman modulation method was used to improve the sensitivity.

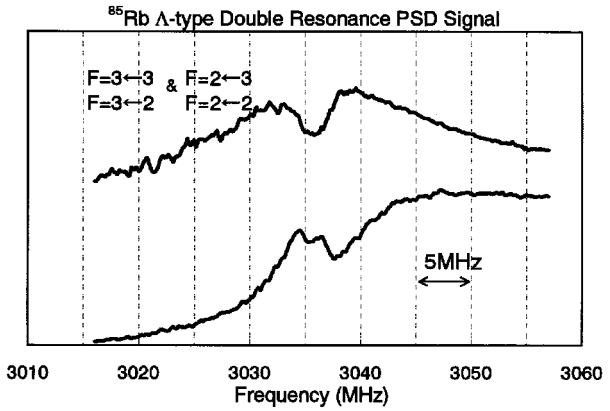

Figure 2. Cosine and sine components of the optical beat obtained by phase sensitive detection of the double resonance spectrum of ^{85}Rb around 3.035 GHz. The upper and lower signals correspond to the imaginary and real parts of the third-order susceptibility, respectively.